



Advances in computerized MRI-based biomarkers in Alzheimer's disease

Raymond Wong

BrainNow Research Institute, Shenzhen 518081, Guangdong, China

Yishan Luo

BrainNow Research Institute, Shenzhen 518081, Guangdong, China

Vincent Chung-tong Mok

Department of Medicine and Therapeutics, The Chinese University of Hong Kong, Hong Kong 999077, China

Lin Shi

BrainNow Research Institute, Shenzhen 518081, Guangdong, China; Department of Imaging and Interventional Radiology, The Chinese University of Hong Kong, Hong Kong 999077, China

Follow this and additional works at: <https://dc.tsinghuajournals.com/brain-science-advances>

Recommended Citation

Wong, Raymond; Luo, Yishan; Mok, Vincent Chung-tong; and Shi, Lin () "Advances in computerized MRI-based biomarkers in Alzheimer's disease," *Brain Science Advances*: Vol. 7 : No. 1 , Article 5.

DOI: 10.26599/BSA.2021.9050005

Available at: <https://dc.tsinghuajournals.com/brain-science-advances/vol7/iss1/5>

This Review Article is brought to you for free and open access by Tsinghua University Press: Journals Publishing. It has been accepted for inclusion in Brain Science Advances by an authorized editor of Tsinghua University Press: Journals Publishing.

Advances in computerized MRI-based biomarkers in Alzheimer's disease

Raymond Wong¹, Yishan Luo¹, Vincent Chung-tong Mok², Lin Shi^{1,3} (✉)

¹BrainNow Research Institute, Shenzhen 518081, Guangdong, China

²Department of Medicine and Therapeutics, The Chinese University of Hong Kong, Hong Kong 999077, China

³Department of Imaging and Interventional Radiology, The Chinese University of Hong Kong, Hong Kong 999077, China

ARTICLE INFO

Received: 25 December, 2020

Revised: 8 February, 2021

Accepted: 22 February, 2021

© The authors 2021. This article is published with open access at journals.sagepub.com/home/BSA



Creative Commons Non Commercial CC BY-NC: This article is distributed under the terms of the Creative Commons Attribution-NonCommercial 4.0 License (<http://www.creativecommons.org/licenses/by-nc/4.0/>) which permits non-commercial use, reproduction and distribution of the work without further permission provided the original work is attributed as specified on the SAGE and Open Access pages (<https://us.sagepub.com/en-us/nam/open-access-at-sage>).

KEYWORDS

Alzheimer's disease, magnetic resonance imaging, machine learning, deep learning, biomarkers

ABSTRACT

The use of neuroimaging examinations is crucial in Alzheimer's disease (AD), in both research and clinical settings. Over the years, magnetic resonance imaging (MRI)-based computer-aided diagnosis has been shown to be helpful for early screening and predicting cognitive decline. Meanwhile, an increasing number of studies have adopted machine learning for the classification of AD, with promising results. In this review article, we focus on computerized MRI-based biomarkers of AD by reviewing representative studies that used computerized techniques to identify AD patients and predict cognitive progression. We categorized these studies based on the following applications: (1) identifying AD from normal control; (2) identifying AD from other dementia types, including vascular dementia, dementia with Lewy bodies, and frontotemporal dementia; and (3) predicting conversion from NC to mild cognitive impairment (MCI) and from MCI to AD. This systematic review could act as a state-of-the-art overview of this emerging field as well as a basis for designing future studies.

1 Introduction

Alzheimer's disease (AD), the most common type of dementia, is a progressive disease characterized by memory loss and overall cognitive decline beyond normal aging. The prevalence of dementia is increasing worldwide, and in 2016, it became the fifth leading cause of global deaths, as per the World Health

Organization (WHO) statistics [1]. According to the *World Alzheimer Report 2018*, published by Alzheimer's Disease International, there are at least 50 million people worldwide living with AD or other dementias, and that number is expected to triple to 152 million by 2050 [2].

In 2011, the National Institute on Aging and Alzheimer's Association (NIA-AA) began incorporating the use of biomarkers in the diagnostic

Address correspondence to Lin Shi, shilin@cuhk.edu.hk

Abbreviations

3D	three-dimensional	LEAP	learning embeddings for atlas propagation
AD	Alzheimer's disease	LPBM	linear programming boosting method
ADNI	Alzheimer's Disease Neuroimaging Initiative	LR	logistic regression
AD-RAI	AD resemblance atrophy index	LSR	large-scale regularization
AE	autoencoders	MCI	mild cognitive impairment
aMCI	amnestic mild cognitive impairment	MIRIAD	Minimal Interval Resonance Imaging in Alzheimer's Disease
ANFIS	adaptive neuro-fuzzy inference system	MR	magnetic resonance
ANN	artificial neural network	MXD	mixed VD-AD
AUC	area under the curve	NC	normal control
BS	Bayes statistics	ncMCI	mild cognitive impairment nonconverter
bvFTD	behavioral variant FTD	ncNC	normal control nonconverter
CBF	cerebral blood flow	NIA-AA	National Institute on Aging and Alzheimer's Association
CD	cognitively declining	NN	neural network
cMCI	MCI converter	OPLS	orthogonal projection to latent structures
cNC	NC converter	OR	odd ratio
CNN	convolutional neural network	PCA	principal component analysis
CS	cognitively stable	PET	positron emission tomography
CSF	cerebrospinal fluid	RAVENS	regional analysis of volumes examined in normalized space
DBM	deep Boltzmann machine	RBF	radial basis function
DBN	deep belief network	RBM	restricted Boltzmann machine
DLB	dementia with Lewy bodies	RLR	regularized logistic regression
DNN	deep neural network	RNN	recurrent neural network
DTI	diffusion tensor imaging	ROC	receiver-operating characteristic
eMCI	early mild cognitive impairment	RVM	relevance vector machines
EN-RLR	elastic net regularized logistic regression	SAE	stacked autoencoder
EOAD	early-onset Alzheimer's disease	SD	standard deviation
FA	fractional anisotropy	SEN	sensitivity
FDG-PET	2-[fluorine-18]fluoro-2-deoxy-D-glucose PET	SGD	stochastic gradient descent
fMRI	functional magnetic resonance imaging	sMRI	structural magnetic resonance imaging
FTD	frontotemporal dementia	SPARE-AD	Spatial Pattern of Abnormality for Recognition of Early Alzheimer's disease
GAN	generative adversarial networks	SPE	specificity
GM	gray matter	SPLS	sparse partial least squares
HMM	hidden Markov model	sVD	subcortical vascular dementia
iNPH	idiopathic normal pressure hydrocephalus	SVM	support vector machine
IWG	International Working Group	VaD	vascular dementia
LDA	linear discriminant analysis	VFI	voting features intervals
IMCI	late mild cognitive impairment	WHO	World Health Organization
LOO-CV	leave one-out cross-validation	WMH	white matter hyperintensities

criteria of AD [3]. In 2014, the International Working Group (IWG) issued a revised diagnostic criteria IWG-2, which further categorized the biomarkers into diagnostic and progression biomarkers [4], among which tau and amyloid- β positron emission tomography (tau-PET and A β -PET) are used for diagnosis, whereas brain structural magnetic resonance imaging (sMRI) and glucose metabolism imaging (2-[fluorine-18]fluoro-2-deoxy-D-glucose PET, or FDG-PET) are used for monitoring the progression of the disease. In 2018, the NIA-AA published the AT(N) research framework, which proposed three groups of biomarkers: A β deposition (A, based on cerebrospinal fluid [CSF] or A β -PET), pathologic tau (T, based on CSF phosphorylated tau [p-tau] or tau-PET), and neurodegeneration (N, based on FDG-PET, CSF total tau [t-tau], or brain atrophy as measured by MRI), which collectively define the various stages of AD progression [5]. Although the 2018 NIA-AA framework was not intended for clinical diagnosis, it further emphasized the importance of medical imaging for monitoring disease progression and its prospect in early screening for AD. Apart from the core biomarkers, emerging CSF and blood biomarkers such as neurofilament light protein, neuron-specific enolase, and visinin-like protein 1 might be feasible for detecting AD-related neurodegeneration [6]. Other imaging modalities such as diffusion tensor imaging (DTI) [7], arterial spin labeling [8], and functional MRI (fMRI) [9] have also shown great prospects in the research of preclinical AD.

In this review article, we focus on the following aspects of computerized MRI-based biomarkers of AD: (1) identifying AD from normal control (NC), (2) identifying AD from other dementia types, including vascular dementia (VaD), dementia with Lewy bodies (DLB), and frontotemporal dementia (FTD), and

(3) predicting the conversion from NC to mild cognitive impairment (MCI) and from MCI to AD.

2 MRI biomarkers used in identifying AD from NC

With regard to the algorithms used for identifying AD from NC, research has been conducted on machine learning, deep learning, or a combination of both approaches. In some studies, modalities other than MRI, such as PET and cerebrospinal fluid (CSF), were also integrated into the AD/NC classification. Most studies used sMRI as the magnetic resonance (MR) modality. Among these sMRI studies, density maps, cortical surface, and predefined region-based methods were the main extraction methods used in machine-learning studies, whereas the image patch-based method is another common method used in deep-learning studies.

2.1 AD/NC classification using machine learning

In their review, Rathore et al. [10] categorized the MRI-based AD classification studies into sMRI, fMRI, and DTI.

For the sMRI biomarkers of AD, the hippocampus has always played an important role and is considered to be a crucial region that aids in the diagnosis of AD. In particular, hippocampal volume has been validated and accepted by the Coalition Against Major Diseases/European Medicines Agency as the neuroimaging biomarker for trials targeting predementia stages [11]. In addition, other regions have shown significant atrophy or volumetric differences between AD and NC [12, 13]. Therefore, studies using predefined region-based methods have used hippocampal features and biologically selected features beyond the

hippocampus for classification.

Using spherical harmonics to model the shape of the hippocampus, Gerardin et al. [14] detected an accuracy of 94% for the classification of AD/NC. Li et al. [15] quantified the hippocampal shape using surface-based anatomic mesh modeling and reported an accuracy of 94.9%. After constructing a statistical shape model for the hippocampus, She et al. [16] reported an accuracy of 88.3%. Wang et al. [17] demonstrated an accuracy of 81.1% using a large-deformation diffeomorphic and momentum-based hippocampal shape. Sørensen et al. [18] used hippocampal texture to yield an area under the curve (AUC) of 0.912 in discriminating AD from NC.

Among studies using biologically selected features beyond the hippocampus, Chincarini et al. [19] achieved an AUC of 0.97 using temporal lobe structures that are known to be affected in early AD, such as the entorhinal cortex, perirhinal cortex, hippocampus, and parahippocampal gyri. In addition, Spulber et al. [20] used supervised multivariate data analysis and orthogonal projection to latent structures (OPLS) for statistical learning, yielded an accuracy of 88.4% for the AD/NC classification using cortical thickness and volumetric features. In a more recent study, Mai et al. [21] combined the degree of atrophy of multiple brain structures into an AD resemblance atrophy index (AD-RAI) and evaluated its performance among groups of AD/NC and subgroups of AD/NC that were assessed with AT(N) biomarkers and demonstrated accuracies of 91% and 100%, respectively.

In addition to predefined region-based methods, density maps and cortical surface are other main feature extraction methods that can be used in sMRI for AD/NC classification. In studies using the density map-based method,

researchers used either whole-density maps [22–27] or reduced-density maps as features, which are features that have been reduced using supervised or unsupervised feature-reduction methods [28–30] or features that have been extracted from predefined atlases [31] or adaptive regions to reduce dimensionality [32–34]. For studies using the surface-based method, the authors used supervised/unsupervised feature reduction-based methods [35, 36] or atlas-based methods to reduce vertices as features [37–42].

For fMRI studies distinguishing AD from NC, the authors used features that were based on graph theory-based measures [43] or functional connectivity [44]. In the DTI studies, features were extracted based on tractography [45], connectivity network measures [46], and discriminative voxel selection [47].

Table 1 presents a summary of MRI studies for identifying AD from NC.

2.2 AD/NC classification using deep learning for feature selection from neuroimaging data

In the systematic review by Jo et al. [48], the authors identified studies combining traditional machine learning and deep learning, with the latter responsible for the feature selection from the images (Table 2). By using the gray matter (GM) tissue volume from MRI, as well as the mean intensity from PET and CSF biomarkers of A β 42, t-tau, and p-tau as features, Suk et al. [49] used a stacked autoencoder (SAE) to discover a latent feature representation and adopted a multikernel support vector machine (SVM) for classification to achieve an accuracy of 95.9%. These same authors [50] used a deep Boltzmann machine (DBM) to demonstrate an accuracy of 95.35% by using the tissue densities of an MRI patch and the voxel intensities of a PET patch as observations. Later, they combined SAE-learned

Table 1 Summary of studies on AD/CN classification using machine learning. cMCI/ncMCI classification performance is shown when applicable.

Study	MR modality	Classifier	AD/NC accuracy	AD	CN	cMCI/ncMCI accuracy	cMCI	ncMCI
Kloppel et al. (2008)[22]	sMRI (density map based)	SVM	95	20	20			
	sMRI (density map based)	SVM	92.9	14	14			
	sMRI (density map based)	SVM	81.1	33	57			
Casanova et al. (2011) [23]	sMRI (density map based)	LSR	85.7	49	49			
Hinrichs et al. (2009) [24]	sMRI (density map based)	LPBM	82	89	94			
Termenon & Graña (2012) [25]	sMRI (density map based)	RVM, SVM	83	49	49			
Plant et al. (2010) [26]	sMRI (density map based)	SVM, BS, VFI	92	32	18	75	9	15
Möller et al. (2016) [27]	sMRI (density map based)	SVM	88	84	94			
Liu et al. (2013) [28]	sMRI (density map based)	RLR, SVM, LDA	90	86	137	68	97	93
Salvatore et al. (2015) [29]	sMRI (density map based)	SVM	76	137	162	66	76	134
Beheshti & Demirel (2015) [30]	sMRI (density map based)	SVM	89.65	130	130			
Magnin et al. (2009) [31]	sMRI (density map based)	SVM	94.5	16	22			
Fan et al. (2008) [32]	sMRI (density map based)	SVM	94.3	56	66			
Min et al. (2014) [33]	sMRI (density map based)	SVM	91.64	97	128	72.41	117	117
Liu et al. (2015) [34]	sMRI (density map based)	SVM	92.51	97	128	78.88	117	117
Cho et al. (2012) [35]	sMRI (surface based)	LDA	88.33	128	160	71.21	72	131
Park et al. (2012) [36]	sMRI (surface based)	SVM	90	25	50			
Desikan et al. (2009) [37]	sMRI (surface based)	LR	95	65	94			
McEvoy et al. (2009) [38]	sMRI (surface based)	LDA	89	84	139			
Oliveira et al. (2010) [39]	sMRI (surface based)	SVM	88.2	14	20			
Eskildsen et al. (2013) [40]	sMRI (surface based)	LDA	86.7	194	226	71.1	340	134
Wee et al. (2013) [41]	sMRI (surface based)	Multikernel SVM	92.35	198	200	75.05	89	111
Lillemark et al. (2014) [42]	sMRI (surface based)	LDA	87.70 (AUC)	114	170			
Wang et al. (2007) [17]	sMRI (predefined region based)	LR	81.1	18	26			
Li et al. (2007) [15]	sMRI (predefined region based)	SVM	94.9	19	20			
Gerardin et al. (2009) [14]	sMRI (predefined region based)	SVM	94	23	25			
Shen et al. (2012) [16]	sMRI (predefined region based)	Bagged SVM	88.3	99	138			
Sørensen et al. (2016) [18]	sMRI (predefined region based)	SVM	91.20 (AUC)	101	169	74.20 (AUC)	93	140
Chincarini et al. (2011) [19]	sMRI (predefined region based)	SVM	97.00 (AUC)	144	189	74.00 (AUC)	136	166
Mai et al. (2021) [21]	sMRI (predefined region based)	ROC	91	50	50			
Chen et al. (2011) [44]	fMRI	Fisher LDA	82.00	20	20			
Khazaei et al. (2015) [43]	fMRI	SVM	100	20	20			
Nir et al. (2015) [45]	DTI	SVM	80.6	37	50			
Prasad et al. (2015) [46]	DTI	SVM	78.2	38	50	63.4	38	74
Dyrba et al. (2013) [47]	DTI	SVM	83	137	143			

Table 2 Summary of studies on the prediction of NC-to-MCI or MCI-to-AD conversion. AD/NC classification performance is shown when applicable.

Study	MR modality	Other modality	Machine learning/deep learning	Data processing/training	Classifier	AD/NC accuracy	cMCI/ncMCI accuracy	Groups
Suk & Shen (2013) [49]	sMRI (density map based)	PET, CSF	Hybrid	SAE	SVM	95.9	75.8	51 AD 43 cMCI 56 ncMCI 52 NC
Suk et al. (2014) [50]	sMRI (image patch based)	PET	Hybrid	DBM	SVM	95.35	75.92	93 AD 76 cMCI 128 ncMCI 101 NC
Li et al. (2015) [52]	sMRI (predefined region based)	PET, CSF	Hybrid	RBM + dropout	SVM	91.4	57.4	51 AD 43 cMCI 56 ncMCI 52 NC
Suk et al. (2015) [51]	sMRI (predefined region based)	PET, CSF	Hybrid	SAE + sparse learning	SVM	98.8	83.3	51 AD 43 cMCI 56 ncMCI 52 NC
Liu et al. (2014) [53]	sMRI (predefined region based)	PET	Pure deep learning	SAE + NN	Softmax	87.76		65 AD 67 cMCI 102 ncMCI 77 NC
Li et al. (2014) [61]	sMRI (density map based)	PET	Pure deep learning	3D CNN	Logistic regression	92.87		198 AD 167 cMCI 236 ncMCI 229 NC
Liu et al. (2015) [54]	sMRI (predefined region based)	PET	Pure deep learning	SAE with zero masking	Softmax	91.4		77 AD 67 cMCI 102 ncMCI 85 NC
Cheng et al. (2017) [56]	sMRI (image patch based)		Pure deep learning	3D CNN	Softmax	87.15		199 AD, 229 NC
Cheng & Liu (2017) [57]	sMRI (image patch based)	PET	Pure deep learning	3D CNN + 2D CNN	Softmax	89.64		93 AD, 100 NC
Aderghal et al. (2017) [59]	sMRI (predefined region based)		Pure deep learning	2D CNN	Softmax	91.41		188 AD 399 MCI 228 NC
Korolev et al. (2017) [58]	sMRI (image patch based)		Pure deep learning	3D CNN	Softmax	80		50 AD 43 IMCI 77 eMCI 61 NC
Vu et al. (2017) [62]	sMRI (image patch based)	PET	Pure deep learning	SAE + 3D CNN	Softmax	91.14		145 AD 172 NC
Liu et al. (2018) [60]	sMRI (image patch based)		Pure deep learning	Landmark detection + 3D CNN	Softmax	91.09	76.9	159 AD 38 cMCI 239 ncMCI 200 NC
Lu et al. (2018) [55]	sMRI (image patch region based)	PET	Pure deep learning	DNN + NN	Softmax	84.6	82.93	238 AD 217 cMCI 409 ncMCI 360 NC
deToledo-Morrell et al. (2004) [79]	sMRI (predefined region based)		Machine learning	Self-developed volume quantification protocol	Multivariate logistic regression		93.5	10 cMCI 17 ncMCI

(To be continued on the next page)

(Continued)

Study	MR modality	Other modality	Machine learning/deep learning	Data processing/training	Classifier	AD/NC accuracy	cMCI/ncMCI accuracy	Groups
Clerx et al. (2013) [80]	sMRI (predefined region based)		Machine learning	Manual and automated atlas-based segmentation	ROC		0.71 (AUC for manual hippocampus) 0.71 (AUC for LEAP hippocampus)	30 cMCI 126 ncMCI (dataset 1) 61 cMCI 111 ncMCI (dataset 2)
Misra et al. (2009) [81]	sMRI (predefined region based)		Machine learning	RAVENS	High-dimensional pattern classification		81.5	27 cMCI 76 ncMCI
Spulber et al. (2013) [20]	sMRI (predefined region based)		Machine learning	FreeSurfer	Supervised multivariate data analysis, statistical learning (OPLS)	88.4	67.7	295 AD 173 cMCI 261 ncMCI 335 NC
Zhao et al. (2019) [82]	sMRI (predefined region based)		Machine learning	AccuBrain	ROC		0.771 (AUC) 0.740 (cNC/ncNC AUC)	25 AD 35 cMCI 50 ncMCI 23 cNC 50 ncNC
Davatzikos et al. (2009) [68]	sMRI (predefined region based)		Machine learning	RAVENS	High-dimensional pattern classification	0.885 (MCI/NC AUC)		56 AD 66 NC (Training), 15 ncMCI 109 NC (Testing)
Clark et al. (2012) [85]	sMRI (predefined region based)	PET, CBF	Machine learning	RAVENS (MRI processing)	SVM (High-dimensional pattern classification)		86 (CS/CD)	143 NC (25 CS, 25 CD)
Bangen et al. (2018) [83]	sMRI (predefined region based)		Machine learning	Manual and multiatlas segmentation (WMH as quartiles)	Logistic regression		2.04 (cNC/ncNC OR)	489 ncNC 72 cNC
				Manual and multiatlas segmentation (hippocampal volume as quartiles)			2.13 (cNC/ncNC OR)	489 ncNC 72 cNC
				Manual and multiatlas segmentation (total brain volume change rate as quartiles)			3.03 (cNC/ncNC OR)	435 ncNC 56 cNC
				Manual and multiatlas segmentation (continuous hippocampal volume change rate)			0.68 (cNC/ncNC OR)	449 ncNC 42 cNC (conversion to aMCI)

feature representation with the original low-level features from multimodality fusion via multikernel SVM and showed the highest accuracy of 98.8% in semisupervised learning [51]. Li et al. [52] used volumetric features from MRI and PET images and CSF biomarkers of A β 42, t-tau, and p-tau, via the restricted Boltzmann machine (RBM) with dropout and SVM as a classifier, to obtain an accuracy of 91.4%.

2.3 Deep learning for classification of AD and NC

Jo et al. [48] also identified several studies that used only deep learning for identifying AD from NC (Table 2). Liu et al. [53] used SAE and a softmax output layer to yield an accuracy of 87.76% for the classification of AD/NC. Liu et al. [54] proposed a framework using SAE and a softmax logistic regressor and applied a zero-mask method to achieve an accuracy of 91.4%. Lu et al. [55] used a deep neural network (DNN) and obtained an accuracy of 84.6%. Cheng et al. [56] proposed the construction of multiple deep three-dimensional (3D) convolutional neural networks (CNNs) and reported an accuracy of 87.15%. Later, they proposed the construction of cascaded CNNs (3D CNN + 2D CNN) and achieved an accuracy of 89.64% [57]. Using residual and plain 3D CNN architectures without intermediate handcrafted feature extraction, Korolev et al. [58] reported an accuracy of 80%. Aderghal et al. [59] proposed a multiprojection fusion approach using CNNs and demonstrated an accuracy of 91.41%. Liu et al. [60] proposed a landmark-based deep multi-instance learning framework to achieve accuracies of 91.09% and 92.75% from the Alzheimer's Disease Neuroimaging Initiative (ADNI)-2 and Minimal Interval Resonance Imaging in Alzheimer's Disease (MIRIAD), respectively. Li et al. [61] designed a 3D CNN

architecture and yielded an accuracy of 92.87%. Vu et al. [62] used SAE and 3D CNN and demonstrated an accuracy of 91.1%.

3 MRI biomarkers in differentiating AD from other dementia types

Table 3 provides a list of studies classifying AD versus DLB, FTD, and VaD. All of the examined studies used machine learning to differentiate AD from other dementia types. The MR modalities used in these studies include sMRI, DTI, and fMRI.

3.1 Classification between AD and DLB

One of the supportive biomarkers, according to the 2017 revised criteria for the clinical diagnosis of DLB, is a relative preservation of medial temporal lobe structures on computed tomography or MRI scan [63]. To differentiate DLB from AD, Matsuda et al. [64] investigated the local atrophy of the medial temporal lobe and brainstem and reported accuracies of 73.4% and 63.3% in the receiver-operating characteristic (ROC) analyses for the training and testing sets, respectively. Lebedev et al. [65] used the sparse partial least squares regression (SPLS) classification using cortical thickness and achieved AUCs of 0.948 and 0.731 for the training and testing sets, respectively.

3.2 Classification between AD and FTD

To differentiate AD from FTD, Kim et al. [66] used principal component analysis (PCA) and linear discriminant analysis (LDA) classifiers and achieved an accuracy of 90.8% based on cortical thickness. By using the GM density map as a feature, Möller et al. [27] used SVM for the classification to show a training accuracy of 79%, whereas single-subject diagnosis in the prediction set yielded 82% accuracy when using the

Table 3 Summary of studies on the classification between AD and other types of dementia.

Study	Type of non-AD dementia	MR modality	Classifier	AD/non-AD accuracy	Groups
Lebedev et al. (2013) [65]	DLB	sMRI (surface based)	SPLS	0.731 (testing AUC), 0.948 (training AUC)	97 DLB, 97AD
Matsuda et al. (2019) [64]	DLB	sMRI (predefined region based)	ROC	63.3 (testing AUC), 73.4 (training AUC)	239 DLB, 385 AD (414 training, 210 testing)
Kim et al. (2019) [66]	FTD	sMRI (surface based)	PCA + LDA hierarchical classification	90.8 (FTD/AD), 75.8 (overall)	143 FTD, 50AD, 146 NC
Möller et al. (2016) [27]	FTD	sMRI (density map based)	SVM	79 (training), 82 (single subject)	84 AD, 51 bvFTD, 94 NC (training: 42 AD, 26 bvFTD, 47 NC; testing: 42 AD, 25 bvFTD, 47 NC)
Raamana et al. (2014) [67]	FTD	sMRI (predefined region based)	SVM + RBF kernel	65 (train/test), 72 (LOO-CV)	34 AD, 30 bvFTD, 14 NC
Davatzikos, et al. (2008) [68]	FTD	sMRI (predefined region based)	SVM	84.3	37 AD, 37 NC; 12 FTD, 12 NC
Du et al. (2007) [69]	FTD	sMRI (surface based)	LOO-CV of the logistic regressions	82	23 NC, 22 AD, 19 FTD
Canu et al. (2017) [70]	FTD	sMRI (surface based), DTI	Random Forest	82	62 EOAD, 27 bv FTD, 48 NC
Yu et al. (2021) [71]	FTD	sMRI (predefined region based)	ROC	0.93 (AUC)	50 AD, 50 FTD (validation dataset)
Palesi et al. (2018) [73]	VaD	DTI	ROC from stepwise discriminant analysis	75.9	31 AD, 27 VaD, 35 NC
Goujon et al. (2018) [75]	VaD	DTI	ROC	0.995 (AUC)	30 iNPH, 30AD, 30 sVD, 30 NC
Zarei et al. (2009)[74]	VaD	DTI	Discriminant analysis model in stepwise approach	87.5	13 VaD, 16 AD, 22 NC
Zheng et al. (2019) [76]	VaD	sMRI (predefined region based)	SVM + RBF	84.35	58 AD, 35 VaD
Castellazzi et al. (2020) [77]	VaD	fMRI, DTI	ANFIS (best); ANN, SVM	85.25 77.33	33 AD, 27 VD 15 MXD (mixed VD-AD with 3-year follow-up)

discrimination maps. By studying the volume, surface displacement, and Laplacian invariants of the hippocampus and lateral ventricle, Raamana et al. [67] applied k-means clustering for dimensionality reduction and used SVM with radial basis function (RBF) kernel for classification. When using left ventricular displacements as features, these authors reported 72% accuracy from leave-one-out cross-validation (LOO-CV) classification and 65% accuracy from the train/test classification. In addition, they achieved a three-class AUC of 0.76 using bilateral ventricular displacement as features, which is the first multiclass

classification study among AD, FTD, and NC. Using regional analysis of volumes examined in normalized space (RAVENS) for image processing and PCA for feature selection, Davatzikos et al. [68] selected features from different brain regions and reported an accuracy of 84.3% from SVM classification. Du et al. [69] studied the cortical thickness and yielded 82% accuracy from LOO-CV of logistic regression. Canu et al. [70] conducted a multimodal MRI study by combining the cortical thickness and diffusion tensor measures and was able to distinguish patients with early-onset Alzheimer's disease (EOAD) and those with FTD with

82% accuracy from random forest analysis. Recently, by incorporating volumetric indexes in FTD-dominant regions, Yu et al. [71] developed the frontotemporal dementia index and achieved an AUC of 0.93, as validated in independent data from ADNI and the Frontotemporal Lobar Degeneration Neuroimaging Initiative database.

3.3 Classification between AD and VaD

The existence of overlap between pathology of AD and VaD is widely accepted [72]. Therefore, it is crucial to obtain a reliable method of distinguishing these two types of dementia. By using fractional anisotropy (FA) values of multiple regions as features, Palesi et al. [73] classified AD and VaD with 75.9% accuracy from a stepwise discriminant analysis. Zarei et al. [74] showed their highest accuracy of 87.5% from a combined discriminant analysis model based on transcallosal prefrontal FA values and Fazekas score. Goujon et al. [75] achieved their highest AUC of 0.995 using apparent diffusion coefficient values in the parietal periventricular region as features. Zheng et al. [76] used SVM with RBF kernel for classification and yielded an accuracy of 84.35% using structural MRI biomarkers obtained by AccuBrain® as input features. In their recent study, Castellazzi et al. [77] tested three machine-learning algorithms: artificial neural network (ANN), SVM, and adaptive neuro-fuzzy inference system (ANFIS), with both structural and functional information used as input features. When providing multiple regional metrics from resting-state fMRI and DTI as inputs, ANFIS was the most efficient algorithm for discriminating AD from VaD, which yielded an accuracy of 85.25%. In addition, when applying the best discriminant pattern to patients diagnosed with mixed VaD-AD dementia (who converted to AD or VaD at the 3-year follow-up), ANFIS showed

77.33% accuracy in predicting the underlying disease based on the baseline data, which demonstrates the potential for early detection on the typology of dementia.

4 Prediction of cognitive conversion from NC to MCI and from MCI to AD

Although many studies have targeted the identification of MCI subjects at risk of AD, few studies have involved the prediction of conversion from NC to MCI. With regard to the algorithms used for predicting disease progression, machine learning, deep learning, or a combination of both approaches have been reported. sMRI was the mostly used MR modality in the examined studies. Some of the studies mentioned in Section 2 also predicted MCI to AD conversion (Table 1 and Table 2).

4.1 Machine learning for prognostic prediction

Similar to the AD/NC classification, we found that the hippocampus and several AD-related regions were commonly used biomarkers for the prediction of cognitive conversion from MCI to AD. Several predefined region-based studies mentioned in Section 2.1 also applied their classification algorithms to the prediction of the conversion from MCI to AD. Sørensen et al. [18] used hippocampal texture as a predictor of MCI-to-AD conversion and obtained an AUC of 0.742. Chincarini et al. [19] computed a single index combining local analysis of several regions and yielded an accuracy of 0.74. In addition, by quantifying entorhinal volume using their developed protocol, Goncharova et al. [78] and deToledo-Morrell et al. [79] used multivariate logistic regression to achieve their best concordance rate of 93.5% of MCI to AD conversion. Plant et al. [26] investigated the performance of three types of classifier and obtained their best prediction accuracy of 75% of

MCI-to-AD conversion when using voting features intervals (VFI), in which the anterior cingulate gyrus and orbitofrontal cortex were the best features. Clerx et al. [80] studied the use of the hippocampus, medial temporal lobe atrophy score, and lateral ventricle as features and yielded the best AUC of 0.71 using the hippocampus segmented either manually or using the Learning Embeddings for Atlas Propagation (LEAP) method. Misra et al. [81] achieved a prediction accuracy of 81.5% for the MCI-to-AD conversion using a high-dimensional pattern classification of brain atrophy. By using supervised multivariate data analysis and OPLS for statistical learning, Spulber et al. [20] used brain regions segmented from FreeSurfer as features and used AD/CN and cMCI/ncMCI as the training set and testing set, respectively, which yielded an accuracy of 67.7% for the MCI-to-AD conversion. By using their AD-RAI index, which combined the atrophy degree of multiple brain structures, Zhao et al. [82] yielded an AUC of 0.771 for the MCI-to-AD conversion.

In addition to the predefined region-based methods, several density maps and cortical surface-based sMRI studies mentioned in Section 2.1 also applied their classification algorithms in predicting the conversion from MCI to AD. Among the sMRI studies using the density map-based method, Liu et al. [28] used embedded MRI features of regional brain volume and cortical thickness and reported an accuracy of 68%. Salvatore et al. [29] implemented PCA coupled with a Fisher discriminant ratio criterion to MR images (whole-brain, GM, and white matter) and obtained an accuracy of 66%. Min et al. [33] extracted adaptive regional features and yielded an accuracy of 72.41%. Liu et al. [34] proposed a novel view-centralized multiatlas classification method and achieved an accuracy of 78.88% for

cMCI/ncMCI classification. Among the sMRI studies using a cortical surface-based method, Cho et al. [35] demonstrated an accuracy of 71.21% based on the incremental method using a spatial frequency representation of cortical thickness data. Eskildsen et al. [40] used patterns of cortical thickness measurements for the cMCI/ncMCI classification and reported an accuracy of 71.1%. By integrating the correlative morphological information with region of interest-based information via multikernel SVM, Wee et al. [41] achieved an accuracy of 75.05%. Last but not least, among the DTI studies, Prasad et al. [46] reported an accuracy of 63.4% for cMCI/ncMCI classification by combining the fiber network measures and the flow network measures (Table 1).

With regard to the conversion of NC to MCI, Bangen et al. [83] demonstrated that baseline measures of white matter hyperintensities (WMH) and hippocampal volume were associated with a higher odds of conversion from normal cognition to MCI at 6.5-year follow-up. In addition, they found that the annualized change rates in total cerebral brain volume and hippocampal volume were associated with a higher odd of conversion from normal cognition to MCI at follow-up. Using a composite index of multiple MRI features, Zhao et al. [82] reported an AUC of 0.740 for the NC-to-MCI conversion, which demonstrated for the first time that such an index could also differentiate normal subjects at risk of conversion to MCI over a 2-year period. Several other studies also applied a composite index of multiple MRI features to longitudinal data from NC. For instance, by using their spatial pattern of abnormality for the recognition of early Alzheimer's disease (SPARE-AD) index of brain atrophy, Davatzikos et al. [84] evaluated the longitudinal progression of SPARE-AD in NC

and MCI and were able to distinguish these using the rate of SPARE-AD change, which achieved an AUC of 0.89. Later, by combining MRI and resting PET cerebral blood flow (CBF) images, Clark et al. [85] used the resulting index, the spatial pattern of abnormality for recognition of early cognitive decline, to predict subsequent cognitive decline in cognitively normal older adults. Using a combination of MRI and [15O] PET CBF data, they classified cognitively stable (CS) and cognitively declining (CD) individuals with 86% accuracy, using leave-two-out cross-validation. Overall, despite the lack of studies predicting the conversion from NC to MCI using MRI-based biomarkers, it is encouraging that there are multiple ongoing longitudinal studies exploring different neuroimaging biomarkers in people with subjective cognitive decline [86–89].

4.2 Prognostic prediction using deep learning for feature selection from neuroimaging data

The studies mentioned in Section 2.2 also applied their classification algorithms for the prediction of the MCI-to-AD conversion. Suk et al. [49] used the SAE and SVM as classifiers to yield an accuracy of 75.8%. The authors also demonstrated an accuracy of 75.92% in a study using the DBM [50] and an accuracy of 83.3% in another study using SAE [51]. By applying the RBM with a dropout technique, Li et al. [52] obtained an accuracy of 57.4%.

4.3 Deep learning for prognostic prediction

Two of the studies mentioned in Section 2.3 also used pure deep learning for the prediction of MCI to AD conversion. Lu et al. [55] used DNN to yield an accuracy of 82.93% for the MCI-to-AD conversion. Liu et al. [60] used landmark detection and 3D CNN to obtain an accuracy of 76.9%.

5 Discussion

In this review article, we focused on computerized MRI-based biomarkers of AD, for which we identified representative studies using machine learning, deep learning, or a combination of both approaches. Deep learning has the ability to detect complex nonlinear relationships and interactions between variables and has been shown to yield excellent performance in identifying AD from NC and predicting the conversion from MCI to AD. Nonetheless, its black box nature may prevent researchers from clearly understanding its models. In addition, the ability to model nonlinearities and interactions makes deep learning easily prone to overfitting, and training a DNN that generalizes well to new data could be a challenge. Last but not least, deep learning could be much more computationally expensive than machine learning.

Meanwhile, traditional machine learning is relatively better for understanding the effect of features on the classification outcome, which makes it easier to interpret the importance of certain brain features that are extracted from the images. However, for feature extraction and selection, expert knowledge might be required, whereas deep-learning-based classification could be performed using automated selection of features or without feature selection. From this review, we found that traditional machine learning still appears to be widely used in studies of computerized MRI-based biomarkers of AD, ranging from the classification between AD and NC, and between AD and other dementia types, to the prediction of NC-to-MCI and MCI-to-AD conversion.

One of the limitations of this review is that the classification performance metrics of most studies were reported only in terms of accuracy (or AUC when accuracy is not available).

However, a high accuracy does not necessarily indicate good performance. Since these studies had different sample sizes, group composition, and data sets, a fair comparison cannot be made based only on classification accuracy. Thus, when interpreting and comparing the classification performance of different studies, it is essential to consider factors beyond accuracy.

Conflict of interests

Lin Shi is the director of BrainNow Research Institute. Raymond Wong and Yishan Luo are employees of BrainNow Research Institute. The remaining authors report no conflict of interests.

References

- [1] World Health Organization. *Global Health Estimates 2016: Deaths by Cause, Age, Sex, by Country and by Region, 2000–2016*. Geneva: World Health Organization, 2018.
- [2] Alzheimer's Disease International, Patterson C. *World Alzheimer Report 2018 - The State of the Art of Dementia Research: New Frontiers*. London, UK: Alzheimer's Disease International (ADI), 2018, pp 32–36.
- [3] Sperling RA, Aisen PS, Beckett LA, et al. Toward defining the preclinical stages of Alzheimer's disease: recommendations from the National Institute on Aging-Alzheimer's Association workgroups on diagnostic guidelines for Alzheimer's disease. *Alzheimers Dement* 2011, **7**(3): 280–292.
- [4] Dubois B, Feldman HH, Jacova C, et al. Advancing research diagnostic criteria for Alzheimer's disease: the IWG-2 criteria. *Lancet Neurol* 2014, **13**(6): 614–629.
- [5] Jack CR Jr, Bennett DA, Blennow K, et al. NIA-AA Research Framework: Toward a biological definition of Alzheimer's disease. *Alzheimers Dement* 2018, **14**(4): 535–562.
- [6] Olsson B, Lautner R, Andreasson U, et al. CSF and blood biomarkers for the diagnosis of Alzheimer's disease: a systematic review and meta-analysis. *Lancet Neurol* 2016, **15**(7): 673–684.
- [7] Araque Caballero MÁ, Suárez-Calvet M, Duering M, et al. White matter diffusion alterations precede symptom onset in autosomal dominant Alzheimer's disease. *Brain* 2018, **141**(10): 3065–3080.
- [8] Beason-Held LL, Goh JO, An Y, et al. Changes in brain function occur years before the onset of cognitive impairment. *J Neurosci* 2013, **33**(46): 18008–18014.
- [9] Sperling RA, Laviolette PS, O'Keefe K, et al. Amyloid deposition is associated with impaired default network function in older persons without dementia. *Neuron* 2009, **63**(2): 178–188.
- [10] Rathore S, Habes M, Ifitkhar MA, et al. A review on neuroimaging-based classification studies and associated feature extraction methods for Alzheimer's disease and its prodromal stages. *Neuroimage* 2017, **155**: 530–548.
- [11] Hill DLG, Schwarz AJ, Isaac M, et al. Coalition Against Major Diseases/European Medicines Agency biomarker qualification of hippocampal volume for enrichment of clinical trials in prodementia stages of Alzheimer's disease. *Alzheimers Dement* 2014, **10**(4): 421–429.e3.
- [12] Ridha BH, Anderson VM, Barnes J, et al. Volumetric MRI and cognitive measures in Alzheimer disease: comparison of markers of progression. *J Neurol* 2008, **255**(4): 567–574.
- [13] Madsen SK, Ho AJ, Hua X, et al. 3D maps localize caudate nucleus atrophy in 400 Alzheimer's disease, mild cognitive impairment, and healthy elderly subjects. *Neurobiol Aging* 2010, **31**(8): 1312–1325.
- [14] Gerardin E, Chételat G, Chupin M, et al. Multidimensional classification of hippocampal shape features discriminates Alzheimer's disease and mild cognitive impairment from normal aging. *Neuroimage* 2009, **47**(4): 1476–1486.
- [15] Li S, Shi F, Pu F, et al. Hippocampal shape analysis of Alzheimer disease based on machine learning methods. *AJNR Am J Neuroradiol* 2007, **28**(7): 1339–1345.
- [16] Shen KK, Fripp J, Mériaudeau F, et al. Detecting global and local hippocampal shape changes in Alzheimer's disease using statistical shape models. *Neuroimage* 2012, **59**(3): 2155–2166.
- [17] Wang L, Beg F, Ratnanather T, et al. Large

- deformation diffeomorphism and momentum based hippocampal shape discrimination in dementia of the Alzheimer type. *IEEE Trans Med Imaging* 2007, **26**(4): 462–470.
- [18] Sørensen L, Igel C, Liv Hansen N, et al. Early detection of Alzheimer's disease using MRI hippocampal texture. *Hum Brain Mapp* 2016, **37**(3): 1148–1161.
- [19] Chincarini A, Bosco P, Calvini P, et al. Local MRI analysis approach in the diagnosis of early and prodromal Alzheimer's disease. *Neuroimage* 2011, **58**(2): 469–480.
- [20] Spulber G, Simmons A, Muehlboeck JS, et al. An MRI-based index to measure the severity of Alzheimer's disease-like structural pattern in subjects with mild cognitive impairment. *J Intern Med* 2013, **273**(4): 396–409.
- [21] Mai YR, Yu Q, Zhu FQ, et al. AD resemblance atrophy index as a diagnostic biomarker for Alzheimer's disease: a retrospective clinical and biological validation. *J Alzheimers Dis* 2021, **79**(3): 1023–1032.
- [22] Kloppel S, Stonnington CM, Chu C, et al. Automatic classification of MR scans in Alzheimer's disease. *Brain* 2008, **131**(3): 681–689.
- [23] Casanova R, Whitlow CT, Wagner B, et al. High dimensional classification of structural MRI Alzheimer's disease data based on large scale regularization. *Front Neuroinform* 2011, **5**: 22.
- [24] Hinrichs C, Singh V, Mukherjee L, et al. Spatially augmented LPboosting for AD classification with evaluations on the ADNI dataset. *Neuroimage* 2009, **48**(1): 138–149.
- [25] Termenon M, Graña M. A two stage sequential ensemble applied to the classification of Alzheimer's disease based on MRI features. *Neural Process Lett* 2012, **35**(1): 1–12.
- [26] Plant C, Teipel SJ, Oswald A, et al. Automated detection of brain atrophy patterns based on MRI for the prediction of Alzheimer's disease. *Neuroimage* 2010, **50**(1): 162–174.
- [27] Möller C, Pijnenburg YA, van der Flier WM, et al. Alzheimer disease and behavioral variant fronto-temporal dementia: automatic classification based on cortical atrophy for single-subject diagnosis. *Radiology* 2016, **279**(3): 838–848.
- [28] Liu X, Tosun D, Weiner MW, et al. Locally linear embedding (LLE) for MRI based Alzheimer's disease classification. *Neuroimage* 2013, **83**: 148–157.
- [29] Salvatore C, Cerasa A, Battista P, et al. Magnetic resonance imaging biomarkers for the early diagnosis of Alzheimer's disease: a machine learning approach. *Front Neurosci* 2015, **9**: 307.
- [30] Beheshti I, Demirel H, Alzheimer's Disease Neuroimaging Initiative. Probability distribution function-based classification of structural MRI for the detection of Alzheimer's disease. *Comput Biol Med* 2015, **64**: 208–216.
- [31] Magnin B, Mesrob L, Kinkingnéhun S, et al. Support vector machine-based classification of Alzheimer's disease from whole-brain anatomical MRI. *Neuroradiology* 2009, **51**(2): 73–83.
- [32] Fan Y, Batmanghelich N, Clark CM, et al. Spatial patterns of brain atrophy in MCI patients, identified via high-dimensional pattern classification, predict subsequent cognitive decline. *NeuroImage* 2008, **39**(4): 1731–1743.
- [33] Min R, Wu G, Cheng J, et al. Multi-atlas based representations for Alzheimer's disease diagnosis. *Hum Brain Mapp* 2014, **35**(10): 5052–5070.
- [34] Liu MX, Zhang DQ, Shen DG, et al. View-centralized multi-atlas classification for Alzheimer's disease diagnosis. *Hum Brain Mapp* 2015, **36**(5): 1847–1865.
- [35] Cho Y, Seong JK, Jeong Y, et al. Individual subject classification for Alzheimer's disease based on incremental learning using a spatial frequency representation of cortical thickness data. *Neuroimage* 2012, **59**(3): 2217–2230.
- [36] Park H, Yang JJ, Seo J, et al. Dimensionality reduced cortical features and their use in the classification of Alzheimer's disease and mild cognitive impairment. *Neurosci Lett* 2012, **529**(2): 123–127.
- [37] Desikan RS, Cabral HJ, Hess CP, et al. Automated MRI measures identify individuals with mild cognitive impairment and Alzheimer's disease. *Brain* 2009, **132**(Pt 8): 2048–2057.
- [38] McEvoy LK, Fennema-Notestine C, Roddey JC, et al. Alzheimer disease: quantitative structural neuroimaging for detection and prediction of clinical and structural changes in mild cognitive impairment. *Radiology* 2009, **251**(1): 195–205.

- [39] Oliveira PP Jr, Nitrini R, Busatto G, et al. Use of SVM methods with surface-based cortical and volumetric subcortical measurements to detect Alzheimer's disease. *J Alzheimers Dis* 2010, **19**(4): 1263–1272.
- [40] Eskildsen SF, Coupé P, García-Lorenzo D, et al. Prediction of Alzheimer's disease in subjects with mild cognitive impairment from the ADNI cohort using patterns of cortical thinning. *Neuroimage* 2013, **65**: 511–521.
- [41] Wee CY, Yap PT, Shen DG, et al. Prediction of Alzheimer's disease and mild cognitive impairment using cortical morphological patterns. *Hum Brain Mapp* 2013, **34**(12): 3411–3425.
- [42] Lillemark L, Sørensen L, Pai A, et al. Brain region's relative proximity as marker for Alzheimer's disease based on structural MRI. *BMC Med Imaging* 2014, **14**: 21.
- [43] Khazaee A, Ebrahimzadeh A, Babajani-Feremi A. Identifying patients with Alzheimer's disease using resting-state fMRI and graph theory. *Clin Neurophysiol* 2015, **126**(11): 2132–2141.
- [44] Chen G, Ward BD, Xie CM, et al. Classification of Alzheimer disease, mild cognitive impairment, and normal cognitive status with large-scale network analysis based on resting-state functional MR imaging. *Radiology* 2011, **259**(1): 213–221.
- [45] Nir TM, Villalon-Reina JE, Prasad G, et al. Diffusion weighted imaging-based maximum density path analysis and classification of Alzheimer's disease. *Neurobiol Aging* 2015, **36**(Suppl 1): S132–S140.
- [46] Prasad G, Joshi SH, Nir TM, et al. Brain connectivity and novel network measures for Alzheimer's disease classification. *Neurobiol Aging* 2015, **36**(Suppl 1): S121–S131.
- [47] Dyrba M, Ewers M, Wegrzyn M, et al. Robust automated detection of microstructural white matter degeneration in Alzheimer's disease using machine learning classification of multicenter DTI data. *PLoS One* 2013, **8**(5): e64925.
- [48] Jo T, Nho K, Saykin AJ. Deep learning in Alzheimer's disease: diagnostic classification and prognostic prediction using neuroimaging data. *Front Aging Neurosci* 2019, **11**: 220.
- [49] Suk HI, Shen DG. *Deep Learning-Based Feature Representation for AD/MCI Classification*. *Med Image Comput Assist Interv* 2013, **16**(Pt 2): 583–590.
- [50] Suk HI, Lee SW, Shen D, et al. Hierarchical feature representation and multimodal fusion with deep learning for AD/MCI diagnosis. *Neuroimage* 2014, **101**: 569–582.
- [51] Suk HI, Lee SW, Shen DG, et al. Latent feature representation with stacked auto-encoder for AD/MCI diagnosis. *Brain Struct Funct* 2015, **220**(2): 841–859.
- [52] Li F, Tran L, Thung KH, et al. A robust deep model for improved classification of AD/MCI patients. *IEEE J Biomed Health Inform* 2015, **19**(5): 1610–1616.
- [53] Liu SQ, Liu SD, Cai WD, et al. Early diagnosis of Alzheimer's disease with deep learning. in *2014 IEEE 11th International Symposium on Biomedical Imaging (ISBI)*, Beijing, China, 2014, pp 1015–1018.
- [54] Liu SQ, Liu SD, Cai WD, et al. Multimodal neuroimaging feature learning for multiclass diagnosis of Alzheimer's disease. *IEEE Trans Biomed Eng* 2015, **62**(4): 1132–1140.
- [55] Lu DH, Popuri K, Ding GW, et al. Multimodal and multiscale deep neural networks for the early diagnosis of Alzheimer's disease using structural MR and fdg-pet images. *Sci Rep* 2018, **8**(1): 5697.
- [56] Cheng DN, Liu MH, Fu JL, et al. Classification of MR brain images by combination of multi-CNNs for AD diagnosis. In *Proc SPIE 10420, Ninth International Conference on Digital Image Processing (ICDIP 2017)*, Hongkong, China, 2017, 1042042.
- [57] Cheng DN, Liu MH. CNNs based multi-modality classification for AD diagnosis. In *2017 10th International Congress on Image and Signal Processing, BioMedical Engineering and Informatics (CISP-BMEI)*. Shanghai, China, 2017, pp 1–5.
- [58] Korolev S, Safiullin A, Belyaev M, et al. *Residual and plain convolutional neural networks for 3D brain MRI classification*. In *2017 IEEE 14th International Symposium on Biomedical Imaging (ISBI 2017)*, Melbourne, Australia, 2017, pp 835–838.
- [59] Aderghal K, Benois-Pineau J, Afdel K, et al. *FuseMe: Classification of sMRI images by fusion of Deep CNNs in 2D+ ϵ projections*. In *Proceedings of the 15th International Workshop on Content-Based Multimedia Indexing*, Florence, Italy, 2017.
- [60] Liu MX, Zhang J, Adeli E, et al. Landmark-based deep multi-instance learning for brain disease

- diagnosis. *Med Image Anal* 2018, **43**: 157–168.
- [61] Li RJ, Zhang WL, Suk HI, et al. Deep Learning Based Imaging Data Completion for Improved Brain Disease Diagnosis. In *Medical Image Computing and Computer-Assisted Intervention-MICCAI 2014*. Golland P, et al, Eds. Cham: Springer International Publishing, 2014, pp 305–312.
- [62] Vu TD, Yang HJ, Nguyen VQ, et al. Multimodal learning using convolution neural network and Sparse Autoencoder. In *2017 IEEE International Conference on Big Data and Smart Computing (BigComp)*, Jeju, Korea (South), 2017, pp 309–312.
- [63] Yamada M, Komatsu J, Nakamura K, et al. Diagnostic criteria for dementia with lewy bodies: updates and future directions. *J Mov Disord* 2020, **13**(1): 1–10.
- [64] Matsuda H, Yokoyama K, Sato N, et al. Differentiation between dementia with lewy bodies and Alzheimer's disease using voxel-based morphometry of structural MRI: a multicenter study. *Neuropsychiatr Dis Treat* 2019, **15**: 2715–2722.
- [65] Lebedev AV, Westman E, Beyer MK, et al. Multivariate classification of patients with Alzheimer's and dementia with Lewy bodies using high-dimensional cortical thickness measurements: an MRI surface-based morphometric study. *J Neurol* 2013, **260**(4): 1104–1115.
- [66] Kim JP, Kim J, Park YH, et al. Machine learning based hierarchical classification of frontotemporal dementia and Alzheimer's disease. *Neuroimage Clin* 2019, **23**: 101811.
- [67] Raamana PR, Rosen H, Miller B, et al. Three-class differential diagnosis among alzheimer disease, frontotemporal dementia, and controls. *Front Neurol* 2014, **5**: 71.
- [68] Davatzikos C, Resnick SM, Wu X, et al. Individual patient diagnosis of AD and FTD via high-dimensional pattern classification of MRI. *Neuroimage* 2008, **41**(4): 1220–1227.
- [69] Du AT, Schuff N, Kramer JH, et al. Different regional patterns of cortical thinning in Alzheimer's disease and frontotemporal dementia. *Brain* 2007, **130**(Pt 4): 1159–1166.
- [70] Canu E, Agosta F, Mandic-Stojmenovic G, et al. Multiparametric MRI to distinguish early onset Alzheimer's disease and behavioural variant of frontotemporal dementia. *Neuroimage Clin* 2017, **15**: 428–438.
- [71] Yu Q, Mai YR, Ruan YT, et al. An MRI-based strategy for differentiation of frontotemporal dementia and Alzheimer's disease. *Alzheimers Res Ther* 2021, **13**(1): 23.
- [72] Kalaria RN, Ballard C. Overlap between pathology of Alzheimer disease and vascular dementia. *Alzheimer Dis Assoc Disord* 1999, **13**(Suppl 3): S115–S123.
- [73] Palesi F, De Rinaldis A, Vitali P, et al. Specific patterns of white matter alterations help distinguishing Alzheimer's and vascular dementia. *Front Neurosci* 2018, **12**: 274.
- [74] Zarei M, Damoiseaux JS, Morgese C, et al. Regional white matter integrity differentiates between vascular dementia and Alzheimer disease. *Stroke* 2009, **40**(3): 773–779.
- [75] Goujon A, Mejdoubi M, Purcell Y, et al. Can MRI water apparent diffusion coefficient (ADC) value discriminate between idiopathic normal pressure hydrocephalus, Alzheimer's disease and subcortical vascular dementia? *J Neuroradiol* 2018, **45**(1): 15–22.
- [76] Zheng YN, Guo HM, Zhang LJ, et al. Machine learning-based framework for differential diagnosis between vascular dementia and Alzheimer's disease using structural MRI features. *Front Neurol* 2019, **10**: 1097.
- [77] Castellazzi G, Cuzzoni MG, Cotta Ramusino M, et al. A machine learning approach for the differential diagnosis of alzheimer and vascular dementia fed by MRI selected features. *Front Neuroinform* 2020, **14**: 25.
- [78] Goncharova II, Dickerson BC, Stoub TR, et al. MRI of human entorhinal cortex: a reliable protocol for volumetric measurement. *Neurobiol Aging* 2001, **22**(5): 737–745.
- [79] deToledo-Morrell L, Stoub TR, Bulgakova M, et al. MRI-derived entorhinal volume is a good predictor of conversion from MCI to AD. *Neurobiol Aging* 2004, **25**(9): 1197–1203.
- [80] Clerx L, van Rossum IA, Burns L, et al. Measurements of medial temporal lobe atrophy for prediction of Alzheimer's disease in subjects with mild cognitive impairment. *Neurobiol Aging* 2013, **34**(8): 2003–2013.

- [81] Misra C, Fan Y, Davatzikos C. Baseline and longitudinal patterns of brain atrophy in MCI patients, and their use in prediction of short-term conversion to AD: results from ADNI. *Neuroimage* 2009, **44**(4): 1415–1422.
- [82] Zhao L, Luo YS, Lew D, et al. Risk estimation before progression to mild cognitive impairment and Alzheimer's disease: an AD resemblance atrophy index. *Aging (Albany NY)* 2019, **11**(16): 6217–6236.
- [83] Bangen KJ, Preis SR, Delano-Wood L, et al. Baseline white matter hyperintensities and hippocampal volume are associated with conversion from normal cognition to mild cognitive impairment in the Framingham offspring study. *Alzheimer Dis Assoc Disord* 2018, **32**(1): 50–56.
- [84] Davatzikos C, Xu F, An Y, et al. Longitudinal progression of Alzheimer's-like patterns of atrophy in normal older adults: the SPARE-AD index. *Brain* 2009, **132**(Pt 8): 2026–2035.
- [85] Clark VH, Resnick SM, Doshi J, et al. Longitudinal imaging pattern analysis (SPARE-CD index) detects early structural and functional changes before cognitive decline in healthy older adults. *Neurobiol Aging* 2012, **33**(12): 2733–2745.
- [86] Li X, Wang XN, Su L, et al. Sino Longitudinal Study on Cognitive Decline (SILCODE): protocol for a Chinese longitudinal observational study to develop risk prediction models of conversion to mild cognitive impairment in individuals with subjective cognitive decline. *BMJ Open* 2019, **9**(7): e028188.
- [87] Rodriguez-Gomez O, Sanabria A, Perez-Cordon A, et al. FACEHBI: a prospective study of risk factors, biomarkers and cognition in a cohort of individuals with subjective cognitive decline. study rationale and research protocols. *J Prev Alzheimers Dis* 2017, **4**(2): 100–108.
- [88] Dubois B, Epelbaum S, Nyasse F, et al. Cognitive and neuroimaging features and brain β -amyloidosis in individuals at risk of Alzheimer's disease (INSIGHT-preAD): a longitudinal observational study. *Lancet Neurol* 2018, **17**(4): 335–346.
- [89] Jessen F, Spottke A, Boecker H, et al. Design and first baseline data of the DZNE multicenter observational study on pre-dementia Alzheimer's disease (DELCODE). *Alzheimers Res Ther* 2018, **10**(1): 15.



Lin Shi received the Ph.D. degree from the Department of Computer Science in the Chinese University of Hong Kong (CUHK) in 2008. She was an assistant professor of Neurology in CUHK (2014–2017), and is now an associate professor at the Department of Imaging and Interventional Radiology in CUHK. Her research interests are mainly in the field of multimodal image quantification of brain and orthopedic images to support clinical research and practice. She founded a start-up company, BrainNow Ltd. in 2015 to promote the clinical applications of neuroimaging analysis technology. E-mail: shilin@cuhk.edu.hk

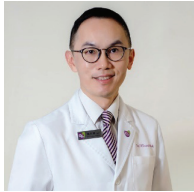


Raymond Wong received the B.Eng. degree from the Department of Biomedical Engineering (BME) of the Chinese University of Hong Kong (CUHK) in 2016 and

then worked as a junior research assistant at the Department of Medicine and Therapeutics in CUHK (2016–2018). He is currently a research assistant at BrainNow Research Institute. He has won the 3rd prize of BME Final Year Project Poster Award 2016 for the project “Fusion of fMRI and EEG brain data”. His main research interest is brain imaging analysis and signal processing. E-mail: raymond.lt.wong@gmail.com



Yishan Luo received her Ph.D. degree from the Hong Kong University of Science and Technology in 2012. She was previously a postdoc research fellow at the Department of Imaging and Interventional Radiology of the Chinese University of Hong Kong (2013–2016), and is currently the R&D manager at BrainNow Research Institute. Her major research interests focus on medical image analysis, image processing and signal processing, in particular, image registration, atlas construction, MRI and DTI analysis and so on. E-mail: lys84818@hotmail.com



Vincent Mok received the M.D. degree from the Chinese University of Hong Kong (CUHK) in 2005. He was the past-president of the Chinese Dementia Research Association (2015–2016), and is currently the Head of Neurology, Division of Neurology, Department of Medicine and Therapeutics, CUHK. His research aims to understand mechanisms of dementia and to investigate strategies that may help to prevent dementia and cerebrovascular disease. Moreover, he also specializes in Parkinson's disease and was one of the pioneers of developing deep brain stimulation programme in the region. E-mail: vctmok@cuhk.edu.hk